THE JOURNAL OF BIOLOGICAL CHEMISTRY
Vol. 278, No. 39, Issue of September 26, pp. 37777–37781, 2003

Printed in U.S.A.

Crystal Structure of von Willebrand Factor A1 Domain Complexed with Snake Venom, Bitiscetin

INSIGHT INTO GLYCOPROTEIN Ibα BINDING MECHANISM INDUCED BY SNAKE VENOM PROTEINS*

Received for publication, May 28, 2003
Published, JBC Papers in Press, July 8, 2003, DOI 10.1074/jbc.M305566200

Nobuo Maita‡§, Kenji Nishio¶, Etsuko Nishimoto‡, Taei Matsui‖, Yasuo Shikamoto‡, Takashi Morita, J. Evan Sadler¶, and Hiroshi Mizuno‡ ‡‡**

*From the ‡Department of Biochemistry, National Institute of Agrobiological Sciences, Tsukuba, Ibaraki 305-8602, Japan, ‖Department of Biology, Fujita Health University School of Health Sciences, Toyoake, Aichi 470-1192, Japan, **Department of Biochemistry, Meiji Pharmaceutical University, Kiyose, Tokyo 204-8588, Japan, and ¶Howard Hughes Medical Institute, Department of Medicine, Washington University School of Medicine, St. Louis, Missouri 63110*

Bitiscetin, a platelet adhesion inducer isolated from venom of the snake *Bitis arietans*, activates the binding of the von Willebrand factor (VWF) A1 domain to glycoprotein Ib (GPIb) *in vitro*. This activation requires the formation of a bitiscetin-VWF A1 complex, suggesting an allosteric mechanism of action. Here, we report the crystal structure of bitiscetin-VWF A1 domain complex solved at 2.85 Å. In the complex structure, helix α5 of VWF A1 domain lies on a concave depression on bitiscetin, and binding sites are located at both ends of the depression. The binding sites correspond well with those proposed previously based on alanine-scanning mutagenesis (Matsui, T., Hamako, J., Matsushita, T., Nakayama, T., Fujimura, Y., and Titani, K. (2002) *Biochemistry* 41, 7939–7946). Against our expectations, the structure of the VWF A1 domain bound to bitiscetin does not differ significantly from the structure of the free A1 domain. These results are similar to the case of botrocetin, another snake-derived inducer of platelet aggregation, although the binding modes of botrocetin and bitiscetin are different. The modeled structure of the ternary bitiscetin-VWF A1-GPIb complex suggests that an electropositive surface of bitiscetin may interact with a favorably positioned anionic region of GPIb. These results suggest that snake venom proteins induce VWF A1-GPIbα binding by interacting with both proteins, and not by causing conformational changes in VWF A1.

Von Willebrand factor (VWF)[1] plays a key role in hemostatic plug formation at sites of vascular injury by interacting with subendothelial matrix proteins and platelet glycoprotein Ib (GPIb) (1). VWF exists as a disulfide-linked multimer composed of identical ~250-kDa subunits, each of which contains three adjacent A domains (A1, A2, and A3). The A1 and A3 domains have major binding sites for GPIb and collagens (types I and III), respectively, and the A2 domain contains the cleavage site for the plasma VWF-cleaving protease (ADAMTS13), which regulates the functional multimer size of VWF (2).

Binding between VWF A1 domain and GPIbα is evident only when blood is exposed to high shear stress *in vivo* (3, 4). This binding activation mechanism is proposed to reflect structural changes in the A1 domain (4, 5). A structural change in the Asp^{560}–Gly^{561} region was observed in the structure of the VWD type 2B "gain-of-function" A1 domain mutant, which binds spontaneously to GPIb under physiological conditions (6). Binding of VWF to platelets *in vitro* occurs in the presence of various modulators, such as the antibiotic ristocetin (7) or snake venom proteins bitiscetin (8) or botrocetin (9). Snakes employ bitiscetin and botrocetin to disrupt hemostasis and thereby to kill or weaken their prey; these modulators have been used extensively as tools to study the complicated mechanisms involved in hemostasis.

Bitiscetin and botrocetin are members of C-type lectin-like proteins (CLPs). The first determination of the complete amino acid sequence of CLPs was carried out using coagulation factors IX- and X-binding protein (IX/X-bp) from *Trimeresurus flavoviridis* (habu snake) venom (10). Up to the present time, various CLPs have been sequenced and characterized with a variety of activities that affect plasma proteins, platelets, endothelial cells, and subendothelial structures. Thus, CLPs with diverse activities appear to be derived from a common ancestor. In this connection, IX/X-bp and IX-bp from habu snake venom have diversified their amino acid sequences in an accelerating manner (11) as also observed for crotalinae snake venom gland phospholipases (12) and serine proteases (13). As shown for the digestive enzymes in venom, which vary predictably in response to differences in diet (14), CLPs have evolved possibly to gain functional diversity in response to important components in the hemostatic system of their prey.

CLPs are heterodimeric proteins consisting of homologous subunits A (α) and B (β) linked by a disulfide bond. Both subunits show a similarity to carbohydrate recognition domains of the classic C-type lectins. The crystal structure of IX/X-bp (15) shows that the two subunits are tightly associated by domain swapping, and this dimerization results in the creation of the concave surface predicted to function as a coagulation factor binding site. Examination of the crystal structure of the complex between X-bp and the γ-carboxyglutamic acid (Gla) domain of factor X has revealed that the binding site is, in fact, the concave surface (16). The structures of CLPs with

* The costs of publication of this article were defrayed in part by the payment of page charges. This article must therefore be hereby marked "*advertisement*" in accordance with 18 U.S.C. Section 1734 solely to indicate this fact.

The atomic coordinates and structure factors (code 1UEX) have been deposited in the Protein Data Bank, Research Collaboratory for Structural Bioinformatics, Rutgers University, New Brunswick, NJ (http://www.rcsb.org/).

§ Present address: Division of Molecular Biophysics, Science of Biological Supramolecular Systems, Yokohama City University, Yokohama, Kanagawa 230-0045, Japan.

‡‡ To whom correspondence should be addressed. Tel.: 81-298-38-7877; Fax: 81-298-38-7408; E-mail: mizuno@affrc.go.jp.

[1] The abbreviations used are: VWF, von Willebrand factor; GPIb, glycoprotein Ib; CLP, C-type lectin-like protein; IX-bp and X-bp, coagulation factors IX-binding protein and X-binding protein.

various functions have been solved by x-ray crystallography (15, 17–20). CLPs have many structural similarities despite having distinct functions, suggesting that electrostatic interactions, as well as size and shape matching, are important for ligand binding.

The concave surfaces of many CLPs have been proposed to form the binding site for a variety of highly diverse ligands. In this connection, we previously showed that the electrostatic potentials on the concave surface are significantly different among IX/X-bp, bitiscetin, and botrocetin (20). Recently, Fukuda *et al.* (21) reported the crystal structure of a botrocetin-VWF A1 complex; they found no large structural change compared with the uncomplexed A1 domain and suggested that the activation of binding by botrocetin is distinct from that of high fluid shear stress. Although bitiscetin and botrocetin have similar effects on VWF function, they are expected to bind VWF A1 quite differently based on the results of alanine scanning studies (22, 23) and also based on the differences in pI and in electrostatic potentials on the concave surface as mentioned above.

To better understand the mechanism by which venom modulators affect hemostasis, we solved the crystal structure of bitiscetin-VWF A1 domain complex. The structure refined at 2.85 Å resolution showed that bitiscetin binds to the A1 domain via its concave surface in a manner different from botrocetin. The bitiscetin contact sites on the A1 domain partially overlapped with those of botrocetin, but the direction of the long-axis of bitiscetin was almost perpendicular to that of botrocetin when the bound A1 domains were superimposed. As in the case of the botrocetin-VWF A1, our structure showed no significant change in the VWF A1 domain. Bitiscetin- and botrocetin-VWF A1 complexes and their electrostatic potential maps revealed a positively charged patch on each venom protein, which is located very close to the anionic region of GPIbα. We propose that this positively charged patch of snake venom modulators plays a key role in the induction of GPIb-binding without inducing a significant conformational change in the GPIb-binding site on VWF.

EXPERIMENTAL PROCEDURES

Materials—Bitiscetin was purified from crude venom of *Bitis arietans* (purchased from ICN Biomedicals Inc.) as described previously (8). Recombinant VWF A1 domain (residues 497–708), expressed in *Escherichia coli* and purified as described (24), was further purified with MonoQ (Amersham Biosciences) and TSK-GEL G2000SW gel filtration column (Tosoh). The affinity of VWF A1 binding to immobilized bitiscetin was measured by a surface plasmon resonance assay using Biacore 3000 (Biacore AB), and a high affinity with a K_d 2 nM was obtained. Bitiscetin and VWF A1 domain were mixed in a 1:1.3 molar ratio, placed on ice for 2–3 h, and then loaded on Superdex 200 column (Amersham Biosciences) equilibrated with sample buffer (10 mM Tris-Cl, pH 7.5, 0.1 M NaCl). Complex-containing fractions were concentrated by ultrafiltration (Microcon, Millipore) to 6 mg/ml. The concentration of protein complex was estimated by absorbance at 280 nm with a molar extinction coefficient of 96,930 liters/mol·cm and a molecular weight of 53,455 for the complex.

Crystallization and Data Collection—Needle-shaped crystals were obtained with a sitting-drop vapor diffusion technique by mixing 3.0 μl of protein solution (6 mg/ml) and 2.5 μl of reservoir solution. The reservoir solution consisted of 88% Crystal Screen II (Hampton Research) no. 30 solution (0.1 M Hepes-Na, pH 7.5, 10% polyethylene glycol 6000, 5% 2-methyl pentanediol) and 12% Crystal Screen II no. 46 solution (0.1 M Bicine-Na, pH 9.0, 20% polyethylene glycol-monomethyl ester 550). The crystals were typically grown to maximum size in 2 weeks at 285 K. A crystal ($0.8 \times 0.15 \times 0.15$ mm^3) was transferred with a nylon loop to cryoprotectant solution consisting of 83% reservoir solution and 17% glycerol and was then rapidly frozen by a cold nitrogen stream at 100 K. Diffraction data were collected at Photon Factory BL-6B (Tsukuba, Japan) with an R-AXIS IV^{++} imaging plate detector (Rigaku). The data were integrated by using MOSFLM (25) followed by scaling with SCALA (26) in the resolution range of 30 to 2.85 Å.

TABLE I
Data collection and refinement statistics

Data collection[a]	
X-ray source	Photon Factory BL-6B
Wavelength (Å)	1.000
Detector	R-AXIS IV^{++}
Space group	$P4_3$
Unit cell (Å)	$a = b = 89.28$, $c = 53.39$
Resolution (Å)	30–2.85 (2.99–2.85)
Completeness (%)	91.6 (91.6)
Observed reflections	51631 (8285)
Unique reflections	9055 (1456)
Redundancy	5.6 (5.7)
$\langle I \rangle / \langle \sigma_I \rangle$	6.2 (2.3)
R_{sym} (%)[b]	10.7 (31.1)
Refinement	
Resolution (Å)	20–2.85
R_{cryst}/R_{free} (%)[c]	19.4/27.6
r.m.s.d.[d] bonds (Å)	0.0052
r.m.s.d. angles (°)	1.21
No. of non-H atoms (protein/water)	3633/40
$\langle B \rangle$ (Å^2) (protein/water)	36.1/19.9
Ramachandran plot (%)[e]	
Most favored	79.4
Allowed	19.9
Disallowed	0.7

[a] Values in parentheses correspond to the outer shell.
[b] $R_{sym} = \Sigma|I - \langle I \rangle|/\Sigma I$, where I is the observed intensity and $\langle I \rangle$ is the average intensity obtained from multiple observations of symmetry-related reflections.
[c] $R_{cryst} = \Sigma_{hkl}||F_o| - |F_c||/\Sigma_{hkl}|F_o|$. 12% of the reflections were excluded for the R_{free} calculation.
[d] r.m.s.d., root-mean-square deviation.
[e] Analyzed with PROCHECK (36).

Diffraction rings from unknown salts were observed in all images at 3.23 Å (data not shown), therefore, the diffraction spots within the 3.30–3.16 Å resolution range were excluded during the data processing. The crystals belong to tetragonal space group $P4_1$ or $P4_3$ with unit cell dimensions of $a = b = 89.28$ Å, $c = 53.39$ Å. The V_M value (27) was calculated to 1.99 Å^3/Da assuming one bitiscetin-VWF A1 complex per asymmetric unit. The data collection statistics are summarized in Table I.

Model Building and Refinement—The initial model was built by the molecular replacement method using bitiscetin (Protein Data Bank entry 1JWI) and wild type VWF A1 domain (Protein Data Bank entry 1AUQ) as search models. Molecular replacement calculations with AMoRe (28) were applied independently using each model in the resolution range of 10 to 4 Å. The highest solution from each model indicated that the space group of the crystal was $P4_3$, with correlation coefficients of 0.353 (VWF A1) and 0.184 (bitiscetin) and R-values of 0.482 (VWF A1) and 0.530 (bitiscetin). Applying the corresponding transformation matrices, a proper bitiscetin-VWF A1 complex model could be easily built. Molecular replacement calculations using the complex gave a correlation coefficient and R -value of 0.693 and 0.331, respectively. Subsequent rigid-body refinement, simulated annealing, and individual B-factor refinement were done with the program CNS (29). After several cycles of refinement, the R-factor and R-free (12% of the reflections) decreased to 19.4 and 27.6%, respectively. The final model includes residues 3–127 (α-subunit) and 3–125 (β-subunit) of bitiscetin, 501–702 of VWF A1 domain, and 40 water molecules. The refinement statistics are summarized in Table I.

Fitting Calculation—Model fitting calculations were done using the program LSQKAB (26). Cα atoms of the A1 domain (residues 509–695) employed for calculation. The coordinates used were: wild type VWF A1 (PDB entry 1AUQ) (30), uncomplexed I546V VWF A1 (Protein Data Bank entry 1IJB) (21), botrocetin-complexed I546V VWF A1 (Protein Data Bank entry 1IJK) (21) and GPIbα-complexed R543Q VWF A1 (Protein Data Bank entry 1M10) (31).

RESULTS AND DISCUSSION

Overall Structure of Bitiscetin-VWF A1 Complex—Bitiscetin, as well as other CLPs, has a heterodimeric structure, and VWF A1 domain binds to the concave surface of bitiscetin (Fig. 1*a*). The concave surface often functions as a ligand-binding site as shown previously for the structure of X-bp complexed with the

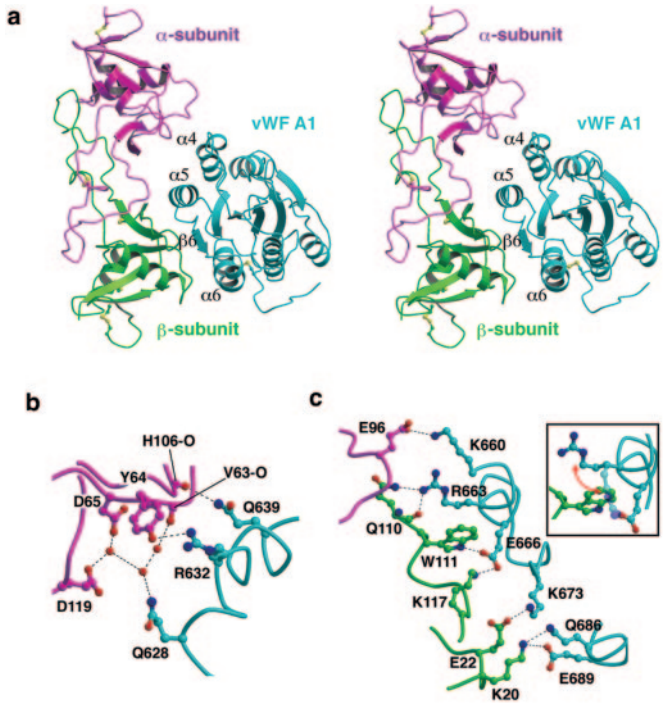

FIG. 1. **Crystal structure of bitiscetin-VWF A1 domain complex.** *a*, stereo-diagram of bitiscetin-VWF A1 domain complex structure. Bitiscetin α-subunit (*magenta*), β-subunit (*green*), and VWF A1 domain (*cyan*) are drawn as *ribbon* representations. Disulfide-bonded cysteine residues are drawn as *ball-and-stick* representations. Helix α4 of A1 contacts the α-subunit of bitiscetin (contact 1), and strand β6 and helices α5 and α6 of A1 contact the β-subunit of bitiscetin (contact 2). *b* and *c*, close-up views of the interaction site between the bitiscetin α-subunit and A1 domain (contact 1) (*b*) and the β-subunit and A1 domain (contact 2) (*c*). Hydrogen bond interactions are shown as *broken lines*. Residues and Cα traces are colored as described in *a*. *c*, *inset*, the *red arrow* shows different positions of Arg^{663} side chains when the A1 domain in the bitiscetin-A1 complex is superimposed on the uncomplexed A1 domain. This figure was generated with MOLSCRIPT (37) and RASTER3D (38).

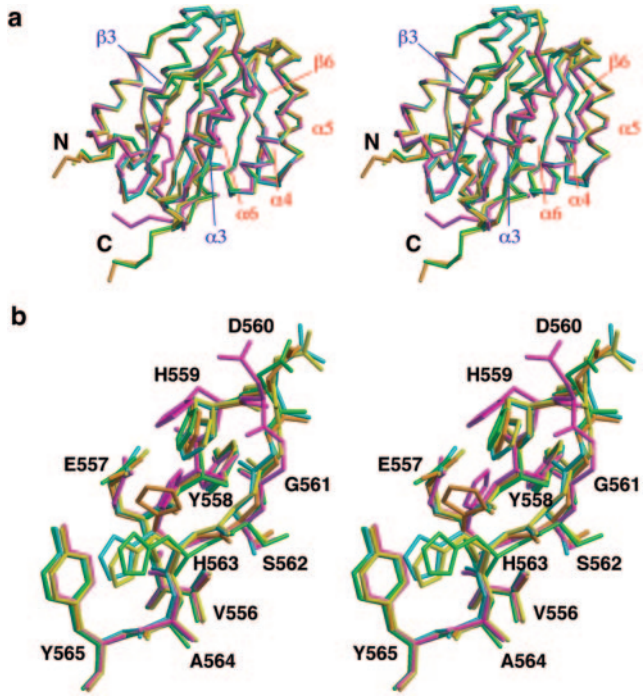

FIG. 2. **Comparison of VWF A1 domain structures.** *a*, stereo-diagram of superimposition of bitiscetin-complexed (*green*), uncomplexed wild type (*gold*), botrocetin-complexed I546V (*cyan*), uncomplexed I546V (*yellow*), and GPIbα-complexed R543Q (*magenta*) VWF A1 structures. Secondary structure elements involved in bitiscetin-binding (*red*) and GPIbα-binding (*blue*) sites are labeled. *b*, stereo-diagram of detailed structure at residues 556–565 of VWF A1 domains. Each model is colored as described in *a*. Uncomplexed I546V (*yellow*) and GPIbα-complexed R543Q (*magenta*) have different conformations for the side chain of Asp^{560}. However, bitiscetin-complexed (*green*), botrocetin-complexed A1 (*cyan*), and uncomplexed wild type (*gold*) A1 have very similar conformations at this site. This figure was generated with MOLSCRIPT (37) and RASTER3D (38).

factor X γ-carboxyglutamic acid domain (16). Helix α5 of the A1 domain is positioned near the center of the concavity, near the junction between the bitiscetin α and β subunit, but interacts mainly with the β-subunit, leaving a solvent-filled space between discontinuous binding sites at both ends of the concave surface of bitiscetin. Helix α4 of the A1 domain contacts the α-subunit of bitiscetin, burying a solvent accessible surface of ~177 $Å^2$, and sheet β6 and helices α5 and α6 contact the β-subunit, burying a solvent accessible surface of ~431 $Å^2$ (Fig. 1*a*).

A comparison with the structure of the botrocetin-VWF A1 complex shows that the botrocetin- and bitiscetin-binding sites overlap at A1 helices α4 and α5. The direction of the long-axis of bitiscetin is almost perpendicular to that of botrocetin when the bound A1 domains are superimposed. Although bitiscetin (516 $Å^2$) and botrocetin (520 $Å^2$) make contact with A1 domains, bitiscetin binds more tightly than botrocetin, with K_d values of 2 and 12 nM (24), respectively. This may be due to a number of solvent-mediated interactions and comfortable fitting of the A1 domain to the concave surface of bitiscetin compared with the case of botrocetin.

Interaction of Bitiscetin and VWF A1 Domain—At the contact region on the α-subunit (contact 1), direct hydrogen bond interactions are observed between Tyr^{64} of bitiscetin and Arg^{632} of the VWF A1 domain (hereafter, the amino acid residues of bitiscetin and VWF A1 will be listed in the same order) and between the main chain carboxyl of His^{106} and Gln^{639}, and indirect water-mediated interactions are observed between Asp^{65} and Gln^{628} and between the O atom of Val^{63} and Asp^{119} (Fig. 1*b*). In the contact region on the β-subunit (contact 2), hydrophobic and hydrogen bond interactions are found. A hydrophobic patch on the β-subunit composed of Leu^{58}, Val^{64}, Leu^{65}, Phe^{104}, and Ile^{109} contacts a hydrophobic surface of the A1 domain that is composed of Pro^{655}, Leu^{659}, Ile^{662}, and Val^{676}. Adjacent to the hydrophobic region, hydrogen bonded interactions are found between Trp^{111} and Lys^{117} in the β-subunit and Glu^{666} in A1, between Gln^{110} and Arg^{663}, between Glu^{22} and Lys^{673}, between Lys^{20} and both Gln^{686} and Glu^{689}, and between Arg^{115} and the backbone oxygens of Glu^{666}, Lys^{667}, and Ala^{669} (Fig. 1*c*). In addition, a hydrogen bond between Glu^{96} in the bitiscetin α-subunit and Lys^{660} in the A1 domain is observed.

Comparison of the Bitiscetin-VWF A1 Structure with Mutagenesis Results—Recently, Matsui *et al.* (23) reported the localization of bitiscetin-binding sites on the VWF A1 domain by alanine-scanning mutagenesis. According to this report, three A1 domain mutations on helix α5 (K660A, E666A, and K673A) and one mutation on helix α4 (R632A) significantly reduced binding to bitiscetin. These results are in good agreement with our structural data, because all of these residues are involved in hydrogen bond interactions with bitiscetin (Fig. 1, *b* and *c*). Interestingly, the A1 mutant R663A showed 1.5-fold higher binding activity relative to the wild type A1 domain (23). The side chain of Arg^{663} interacts with Gln^{110} in the β-subunit of bitiscetin, one of the major interactions between the A1 domain and bitiscetin (Fig. 1*c*), and mutation of Arg^{663} might be expected to reduce the affinity of binding. This contrary result may be explained as follows. The orientation of Arg^{663} in

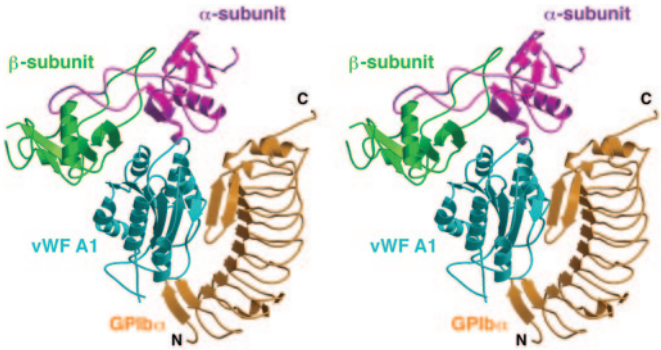

FIG. 3. **Predicted model of bitiscetin-VWF A1-GPIbα ternary complex.** The stereo model was generated from the structures of complexes for bitiscetin-VWF A1 and GPIbα-VWF A1. Bitiscetin α-subunit (*magenta*), β-subunit (*green*), VWF A1 domain (*cyan*), and GPIbα (*gold*) are drawn as *ribbon* representations. This figure was generated with MOLSCRIPT (37) and RASTER3D (38).

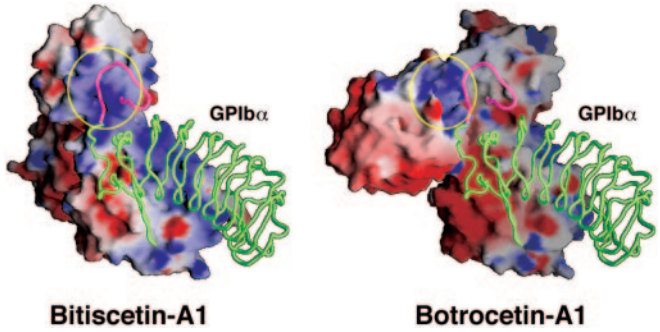

FIG. 4. **Electrostatic surface potentials of the bitiscetin-VWF A1 complex (*left*) and the botrocetin-VWF A1 complex (*right*).** The molecular surface is colored *blue* for a positive charge (+10 kT/e) and *red* for a negative charge (−10 kT/e). GPIbα (Protein Data Bank entry 1M10) models are also shown in a possible bound position in both figures as Cα tube representations (*green*). The C terminus of the GPIbα fragment (residues 264–280), including the anionic region (Protein Data Bank entry 1GWB), is colored in *magenta* for clarity. The positively charged patches on both venom proteins located near the C-terminal anionic region of GPIbα are highlighted with *yellow ovals*. This figure was generated with GRASP (39).

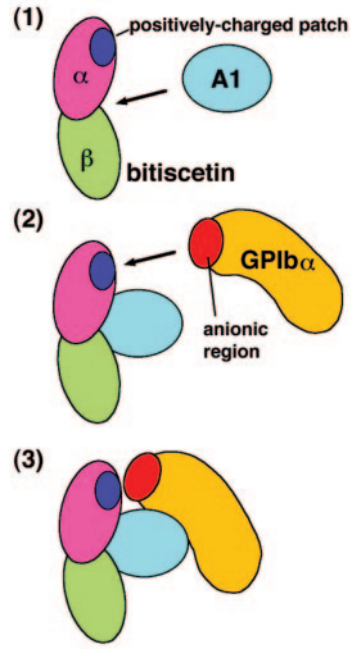

FIG. 5. **Hypothetical model of GPIbα binding activation mechanism induced by bitiscetin.** Step *1* (*top*), The VWF A1 domain (*cyan*) binds to the concave surface of bitiscetin, bringing the GPIbα binding surface of the A1 domain and the positively charged patch on bitiscetin into proximity. Step *2* (*middle*), the anionic region of GPIbα interacts with the positively charged patch of bitiscetin. Step *3* (*bottom*), the anionic region acts as an anchor, which enhances the GPIbα to bind to A1 domain.

bitiscetin-free A1 structure is different from that in the bitiscetin-complexed structure; when A1 domains are superimposed, the Arg^{663} in unbound A1 collides with Trp^{111} of the bitiscetin β-subunit (Fig. 1*c*, *inset*). Moreover, Arg^{663} makes intramolecular hydrogen bonds with Glu^{666} in the free A1 structure that must be broken when bitiscetin binds. Therefore, the mutation R663A may promote binding to bitiscetin by avoiding the need to rearrange the hydrogen bonds and orientation of Arg^{663}, which may be costly in terms of energy.

Comparison with Other von Willebrand Factor A1 Domain Structures—Several studies suggest that structural changes in the A1 domain can increase the affinity of binding to GPIb (4, 5). For example, VWD type 2B mutations in the VWF A1 domain, such as I546V, promote binding to GPIb independent of fluid shear stress (4). The crystal structure of the I546V mutant A1 domain revealed a small structural change in residues Asp^{560}–Gly^{561} at the edge of strand β3 (6, 21), and this change was proposed to cause the increase in affinity for GPIb (6). In the crystal structure of GPIbα-A1 complex, hydrogen bonding interaction are observed between the main chain carboxyl of Asp^{560} and side chain Oγ of Thr^{240} in GPIbα (31), suggesting that the conformation of Asp^{560}–Gly^{561} could change upon GPIbα binding. In the bitiscetin-complexed A1 structure, however, the Asp^{560}–Gly^{561} region has the same conformation as in wild type uncomplexed A1 (Fig. 2*b*). Furthermore, when the wild type or I546V A1 structures were superimposed onto the bitiscetin-complexed A1 structure, no significant structural changes were found at either the bitiscetin- or GPIbα-binding sites (Fig. 2*a*). Large structural changes were observed only in the N-terminal and C-terminal regions of A1 domain that flank the Cys^{509}–Cys^{695} disulfide bond. These regions are expected to be changeable because of their location outside of the disulfide loop, and indeed their flexibility is evident from the crystallographic B-factors in these regions.

Predicted Model of the Bitsicetin-VWF A1-GPIbα Ternary Complex—The crystal structure of the VWF A1 (R543Q)-GPIbα (M239V) complex reveals two binding sites on the A1 domain for GPIb: a major site at the "top" of A1 involves the β3 strand, α3 helix, and part of the α3-β4 loop; a minor site at the "bottom" of the domain involves loops α3-β4, β3-α2, and α1-β2. In the structures of A1 complexed with bitiscetin or botrocetin, however, no significant changes are observed in these regions. Moreover, in the structure of the botrocetin-A1 (I546V) complex, the main chain carboxyl of Asp^{560} has the same conformation as the uncomplexed wild type A1 domain, despite the use of a gain-of-function A1 mutant (21). These observations suggest that bitiscetin and botrocetin stimulate the binding of A1 to GPIb by a mechanism that does not require allosteric conformational changes in VWF A1.

The modeled structure of the bitiscetin-VWF A1-GPIbα ternary complex (Fig. 3) indicates that the binding sites of bitiscetin and GPIbα on the A1 domain do not overlap, so that GPIbα could bind easily to the bitiscetin-VWF A1 complex. In this model, the β-subunit of bitiscetin is well separated from GPIbα, whereas the α-subunit of bitiscetin and the C terminus of the GPIbα fragment are approximated. This model is consistent with the observation that monoclonal antibodies to the α-subunit inhibit GPIb binding to the bitiscetin-A1 complex, but antibodies to the β-subunit do not (23).

Implications for the Mechanism of GPIb-A1 Domain Binding

Induced by Venom Proteins—The electrostatic potential of bitiscetin-A1 complex shows that there is a positively charged patch close to the C terminus of GPIb fragment in the modeled ternary complex (Fig. 4, *left*). The positively charged patch of bitiscetin is constructed from α-subunit residues Lys^{17}, Lys^{20}, Lys^{21}, Lys^{61}, and Lys^{120}. A similar positively charged patch is also found in the botrocetin-A1 complex (Fig. 4, *right*), which consists of α-subunit residues Arg^{98} and Lys^{101} and β-subunit residues Lys^{102}, Lys^{107}, Trp^{109}, Arg^{115}, and Lys^{117} (botrocetin residues are numbered according to Ref. 19). We propose that these positively charged patches observed in both venom proteins are the key to the activation of GPIbα binding to the A1 domain.

At the C terminus of the GPIbα fragment, there is an anionic region (residues 269–279) characterized by three sulfated tyrosine residues, Tyr^{276}, Tyr^{278}, and Tyr^{279} (32). The removal of these sulfate moieties, whether by mutation or by inhibition of sulfation, severely impairs the ability of botrocetin to induce VWF-dependent platelet aggregation (33, 34) indicating that the anionic region of GPIb plays an important role in the high affinity binding of botrocetin-A1 complexes. The anionic region of GPIbα was disordered in the structure of the binary VWF A1-GPIbα complex (31). In the crystal structure of uncomplexed GPIbα, there were two molecules in the asymmetric unit; in one molecule the anionic region was observed but in the other it was disordered (35). These observations suggest that the anionic region of GPIbα is flexible but could adopt a specific conformation upon binding to a nearby positively charged site on bitiscetin or on botrocetin complexed with VWF A1.

Based on their GPIbα-VWF A1 structure, Huizinga *et al.* (31) proposed that the N and C termini of the A1 domain, which are located at the bottom face, shield the binding site from the β-finger of GPIbα. Consequently, structural changes in domain A1 would be necessary for GPIbα binding, and such a requirement for conformational change is consistent with many biochemical and structural studies. However, the crystal structures of the botrocetin-A1 complex (21) and the bitiscetin-A1 complex (Fig. 1) show no significant structural changes in the GPIbα-binding sites of the A1 domain compared with uncomplexed A1. Therefore, the possibility that botrocetin or bitiscetin allosterically activates the A1 domain seems unlikely. We propose that bitiscetin- or botrocetin-induced binding is not dependent on major structural changes of the A1 domain but instead depends mainly on electrostatic interactions between the anionic region of GPIb and a complementary electropositive site contributed by the venom protein in the VWF A1-botrocetin or VWF A1-bitiscetin complex (Fig. 5).

Some experimental data indirectly support this model for botrocetin-induced binding of VWF to GPIb, but the effects of removing sulfated tyrosines or deleting the anionic region of GPIbα have not been studied yet with bitiscetin. For either of these venom proteins, a definitive test of this activation model will require additional biochemical and crystallographic studies of the corresponding ternary complex.

Acknowledgment—We thank Dr. Noriyoshi Sakabe for supporting the data collection at Photon Factory BL-6B.

REFERENCES

1. Sadler, J. E. (1998) *Annu. Rev. Biochem.* **67,** 395–424
2. Chung, D. W., and Fujikawa, K. (2002) *Biochemistry* **41,** 11065–11070
3. Peterson, D. M., Stathopoulos, N. A., Giorgio, T. D., Hellums, J. D., and Moake, J. L. (1987) *Blood* **69,** 625–628
4. Miyata, S., Goto, S., Federici, A. B., Ware, J., and Ruggeri, Z. M. (1996) *J. Biol. Chem.* **271,** 9046–9053
5. Ruggeri, Z. M. (1999) *Thromb. Haemostasis* **82,** 576–584
6. Celikel, R., Ruggeri, Z. M., and Varughese, K. I. (2000) *Nat. Struct. Biol.* **7,** 881–884
7. Hoylaerts, M. F., Nuyts, K., Peerlinck, K., Deckmyn, H., and Vermylen, J. (1995) *Biochem. J.* **306,** 453–463
8. Hamako, J., Matsui, T., Suzuki, M., Ito, M., Makita, K., Fujimura, Y., Ozeki, Y., and Titani, K. (1996) *Biochem. Biophys. Res. Commun.* **226,** 273–279
9. Fujimura, Y., Kawasaki, T., and Titani, K. (1996) *Thromb. Haemostasis* **76,** 633–639
10. Atoda, H., Hyuga, M., and Morita, T. (1991) *J. Biol. Chem.* **266,** 14903–14911
11. Atoda, H., Yoshihara, E., Yamada. M., and Morita, T. (1997) *Thromb. Res.* **87,** 271–278
12. Nakashima, K., Ogawa, T., Oda, N., Hattori, M., Sakaki, Y., Kihara, H., and Ohno, M. (1993) *Proc. Natl. Acad. Sci. U. S. A.* **90,** 5964–5968
13. Deshimaru, M., Ogawa, T., Nakashima, K., Nobuhisa, I., Chijiwa, T., Shimohigashi, Y., Fukumaki, Y., Niwa, M., Yamashina, Y., Hattori, S., and Ohno, M. (1996) *FEBS Lett.* **397,** 83–88
14. Jennifer, C. D., Wolfgang, W., and Roger, S. T. (1996) *Nature* **379,** 537–540
15. Mizuno, H., Fujimoto, Z., Koizumi, M., Kano, H., Atoda, H., and Morita, T. (1997) *Nat. Struct. Biol.* **4,** 438–441
16. Mizuno, H., Fujimoto, Z., Atoda, H., and Morita, T. (2001) *Proc. Natl. Acad. Sci. U. S. A.* **98,** 7230–7234
17. Mizuno, H., Fujimoto, Z., Koizumi, M., Kano, H., Atoda, H., and Morita, T. (1999) *J. Mol. Biol.* **289,** 103–112
18. Fukuda, K., Mizuno, H., Atoda, H., and Morita, T. (2000) *Biochemistry* **39,** 1915–1923
19. Sen, U., Vasudevan, S., Subbarao, G., McClintoc, R. A., Celikel, R., Ruggeri, Z. M., and Varughese, K. I. (2001) *Biochemistry* **40,** 345–352
20. Hirotsu, S., Mizuno, H., Fukuda, K., Qi, M. C., Matsui, T., Hamako, J., Morita, T., and Titani, K. (2001) *Biochemistry* **40,** 13592–13597
21. Fukuda, K., Doggett, T. A., Bankston, L. A., Cruz, M. A., Diacovo, T. G., and Liddington, R. (2002) *Structure* **10,** 943–950
22. Matsushita, T., Meyer, D., and Sadler, J. E. (2000) *J. Biol. Chem.* **275,** 11044–11049
23. Matsui, T., Hamako, J., Matsushita, T., Nakayama, T., Fujimura, Y., and Titani, K. (2002) *Biochemistry* **41,** 7939–7946
24. Miura, S., Li, C. Q., Cao, Z., Wang, H., Wardell, M. R., and Sadler, J. E. (2000) *J. Biol. Chem.* **275,** 7539–7546
25. Leslie, A. G. W. (1999) *Acta Crystallogr. Sect. D Biol. Crystallogr.* **55,** 1696–1702
26. Collaborative Computational Project, Number 4 (1994) *Acta Crystallogr. Sect. D Biol. Crystallogr.* **50**, 760–763
27. Matthews, B. W. (1968) *J. Mol. Biol.* **33,** 491–497
28. Navaza, J. (1994) *Acta Crystallogr. Sect. A* **50**, 157–163
29. Brünger, A. T., Adams, P. D., Clore, G. M., DeLano, W. L., Gros, P., Grosse, R. W.-K., Jiang, J. S., Kuszewski, J., Nilges, M., Pannu, N. S., Read, R. J., Rice, L. M., Simonson, T., and Warren, G. L. (1998) *Acta Crystallogr. Sect. D Biol. Crystallogr.* **54**, 905–921
30. Emsley, J., Cruz, M., Handin, R., and Liddington, R. (1998) *J. Biol. Chem.* **273,** 10396–10401
31. Huizinga, E. G., Tsuji, S., Romijn, R. A., Schiphorst, M. E., de Groot, P. G., Sixma, J. J., and Gros, P. (2002) *Science* **297,** 1176–1179
32. Dong, J., Li, C. Q., and Lopez, J. A. (1994) *Biochemistry* **33,** 13946–13953
33. Marchese, P., Murata, M., Mazzucato, M., Pradella, P., Marco, L., Ware, J., and Ruggeri, Z. M. (1995) *J. Biol. Chem.* **270,** 9571–9578
34. Dong, J., Ye, P., Schade, A. J., Gao, S., Romo, G. M., Turner, N. T., McIntire, L. V., and López, J. A. (2001) *J. Biol. Chem.* **276,** 16690–16694
35. Uff, S., Clemetson, J. M., Harrison, T., Clemetson, K. J., and Emsley, J. (2002) *J. Biol. Chem.* **277,** 35657–35663
36. Laskowski, R. A., MacArthur, M. W., Moss, D. S., and Thornton, J. M. (1993) *J. Appl. Crystallogr.* **26,** 283–291
37. Kraulis, P. J. (1991) *J. Appl. Crystallogr.* **24,** 946–950
38. Merritt, E. A., and Bacon, D. J. (1997) *Methods Enzymol.* **277,** 505–524
39. Nicholls, A., Sharp, K., and Honig, B. (1991) *Proteins* **11,** 281–296

Protein Structure and Folding:

Crystal Structure of von Willebrand Factor A1 Domain Complexed with Snake Venom, Bitiscetin: INSIGHT INTO GLYCOPROTEIN Ib α BINDING MECHANISM INDUCED BY SNAKE VENOM PROTEINS

Nobuo Maita, Kenji Nishio, Etsuko Nishimoto, Taei Matsui, Yasuo Shikamoto, Takashi Morita, J. Evan Sadler and Hiroshi Mizuno

J. Biol. Chem. 2003, 278:37777-37781.
doi: 10.1074/jbc.M305566200 originally published online July 8, 2003
